physics

IMPACT FACTOR 1.8

CITESCORE 3.1

Article

Interacting Ricci-Type Holographic Dark Energy and Dark Sector Couplings

Carlos Rodriguez-Benites, Sergio Santa-María, Nelson Mechán-Zurita, Kenyi Llauce-Baldera, Arnhol Campos-Bocanegra, Cristhian Nunura-Cotrina, Manuel Gonzales-Hernandez, Vaukelyn Viloria-León, Moises Barrios-Cespedes, Fredy Medina-Gamboa et al.

Special Issue

Beyond the Standard Models of Physics and Cosmology: 2nd Edition

Edited by

Prof. Dr. Maxim Y. Khlopov

MDPI

https://doi.org/10.3390/physics8010024

physics

MDPI

Article

Interacting Ricci-Type Holographic Dark Energy and Dark Sector Couplings

Carlos Rodriguez-Benites [1,2,*], Sergio Santa-María [1], Nelson Mechán-Zurita [1], Kenyi Llauce-Baldera [1], Arnhol Campos-Bocanegra [1], Cristhian Nunura-Cotrina [1], Manuel Gonzales-Hernandez [1], Vaukelyn Viloria-León [1], Moises Barrios-Cespedes [1], Fredy Medina-Gamboa [1] and Antonio Rivasplata-Mendoza [2]

[1] GRACOCC (Gravitación, Cosmología, Campos y Cuerdas) Research Group, Facultad de Ciencias Físicas y Matemáticas, Universidad Nacional de Trujillo, Av. Juan Pablo II s/n, Trujillo 13011, Peru; sesamali137@gmail.com (S.S.-M.); nrmechanzu@unitru.edu.pe (N.M.-Z.); krllauceba@unitru.edu.pe (K.L.-B.); akcamposbo@unitru.edu.pe (A.C.-B.); canunuraco@unitru.edu.pe (C.N.-C.); smgonzaleshe@unitru.edu.pe (M.G.-H.); vvviloriale@unitru.edu.pe (V.V.-L.); mbarriosce@unitru.edu.pe (M.B.-C.); f.mega123@gmail.com (F.M.-G.)

[2] Departamento Académico de Física, Facultad de Ciencias Físicas y Matemáticas, Universidad Nacional de Trujillo, Av. Juan Pablo II s/n, Trujillo 13011, Peru; antrivas@unitru.edu.pe

* Correspondence: cerodriguez@unitru.edu.pe

Abstract

We investigate cosmological scenarios in a spatially flat Friedmann–Lemaître–Robertson–Walker (FLRW) universe containing Ricci-type holographic dark energy within the framework of general relativity. The cosmic fluid is composed of baryonic matter, radiation, cold dark matter, and dark energy. We consider three phenomenological interaction schemes in the dark sector and derive analytic expressions for the standard cosmological quantities in each case. Using observational data from cosmic chronometers and Type Ia supernovae (Pantheon sample), we constrain the parameters of the interacting models and determine their best-fit values. Finally, we compare the interacting holographic scenarios with the concordance ΛCDM (Λ cold dark matter) model at the background level, displaying contour plots for the cosmological and interaction parameters and discussing the performance of the models in light of earlier results in the literature.

Keywords: Ricci-type holographic dark energy; dark sector interaction; cosmic chronometers; type Ia supernovae; FLRW cosmology

1. Introduction

Current cosmological observations indicate that the Universe is undergoing an accelerated expansion phase [1–4]. This behavior is usually attributed to a dominant dark energy component that drives the late-time acceleration [5].

The simplest and most studied candidate for dark energy is the cosmological constant Λ, which provides an excellent fit to a wide range of observations within the ΛCDM model. However, the cosmological constant faces known theoretical challenges [6–8]. In particular, the vacuum energy density predicted by quantum field theory exceeds the observed value by many orders of magnitude, and the model does not naturally explain why the current energy densities of dark energy and dark matter are of the same order, despite their very different evolutionary histories. These tensions have motivated a wide class of dynamical dark energy models. Among these, holographic dark energy models are

Check for updates

Received: 14 December 2025
Revised: 3 February 2026
Accepted: 4 February 2026
Published: 1 March 2026

particularly appealing [9–19], as they are rooted in the holographic principle proposed in the context of quantum gravity [20–22].

The holographic principle, conjectured by Gerard 't Hooft [23] and Leonard Susskind [24], states that the physical degrees of freedom inside a given volume can be encoded on its boundary, with the number of degrees of freedom scaling with the area rather than the volume. This idea is closely related to the entropy of a bounded system containing a black hole, as originally discussed by Jacob Bekenstein [25]. In this perspective, the maximal amount of information contained in a spatial region is limited by the area of its boundary [20], and this insight can be translated into constraints on the energy density of the vacuum in a cosmological setting.

In a spatially flat universe, the Ricci scalar of the spacetime is given by

$$\mathcal{R} = 6(\dot{H} + 2H^2), \tag{1}$$

where $H = \dot{a}/a$ is the Hubble expansion rate with a the scale factor, and the dot denotes a derivative with respect to cosmic time t. A specific realization of holographic dark energy based on the Ricci scalar was introduced by Luis Granda and Alexander Oliveros [9]. The corresponding energy density,

$$\rho_x = 3\left(\alpha H^2 + \beta \dot{H}\right), \tag{2}$$

is characterized by two dimensionless constants α and β and has been shown to be in reasonable agreement with observations. This class of models possesses several attractive features [26–28]. In particular, it can fit background data while alleviating, at least partially, the cosmic coincidence problem [10,12–14,29,30]. When the dark energy equation of state ω is allowed to be a function of time, the coincidence parameter $r = \rho_c/\rho_x$, with ρ_c being the cold dark matter density, becomes dynamical and can asymptotically approach a positive constant.

After defining the Ricci-type holographic dark energy density in Equation (2), it is worth clarifying the physical role of the dimensionless constants α and β. In the context of holographic-inspired cosmological models, these parameters are introduced phenomenologically in order to capture possible contributions associated with the local curvature scale of spacetime, encoded through the Hubble parameter H and its first time derivative $\dot{H}$. More specifically, the term proportional to H^2, weighted by the coefficient α, accounts for the dominant contribution related to the expansion rate of the Universe, while the term involving $\dot{H}$, governed by β, incorporates information about the dynamical evolution of the expansion. This structure naturally arises in Ricci-type holographic dark energy scenarios, where the infrared cutoff is associated with the Ricci scalar curvature rather than with the Hubble radius alone [9–11]. In this sense, α and β parametrize deviations from simpler holographic prescriptions and allow for a richer cosmological dynamics at the background level. It is essential to emphasize that, within the scope of the present paper α and β are treated as effective parameters to be constrained by observational data, rather than as fundamental constants derived from an underlying microscopic theory. This phenomenological approach is standard in the literature on Ricci-type holographic dark energy and provides a flexible framework to explore departures from the concordance ΛCDM model while remaining consistent with current cosmological observations.

In this study, we focus on the implications of a Ricci-type holographic dark energy component in the context of modern cosmology, paying special attention to its possible interaction with cold dark matter. We first analyze simplified scenarios with one or two ideal fluids in addition to the holographic component, highlighting under which conditions the model can mimic other fluids or fail to produce a late-time accelerated expansion. We then

turn to a more realistic four-fluid configuration comprising baryons, radiation, cold dark matter, and holographic dark energy and introduce three phenomenological interaction terms in the dark sector. For each interaction scheme, we obtain analytic expressions for the relevant cosmological quantities and confront the models with background data from cosmic chronometers and Type Ia supernovae.

Before proceeding, it is crucial to clarify the conceptual status of the holographic dark energy framework adopted in this study. The use of holographic-inspired energy densities in cosmology is not intended here as a direct implementation of a fundamental quantum–gravitational theory, nor does it assume the existence of a physically observable microscopic granularity of spacetime. Instead, Ricci-type holographic dark energy is employed as an effective phenomenological description of the dark sector at the level of the homogeneous and isotropic cosmological background. In this effective approach, the holographic principle serves as a guiding motivation for constructing infrared cutoffs linked to curvature invariants, such as the Ricci scalar [20–22]. Accordingly, the analysis presented in this paper focuses on the cosmological implications of interacting Ricci-type holographic dark energy at the background level.

The paper is organized as follows. In Section 2, we revisit cosmological scenarios with Ricci-type holographic dark energy in the presence of one or two additional ideal fluids and discuss the emergence of tracking behavior and constant or variable equations of state. Section 3 is devoted to the current four-component scenario, where we introduce the phenomenological interactions in the dark sector and derive the evolution of the dark energy equation of state and the coincidence parameter. In Section 4, we describe the observational data sets and present the constraints on the model parameters, along with a comparison with ΛCDM and previous analyses of holographic models. Finally, in Section 5, we summarize our results and comment on possible extensions of this study.

2. Scenarios with Holography

We consider a homogeneous and isotropic universe within the framework of general relativity, described by the spatially flat Friedmann–Lemaître–Robertson–Walker (FLRW) metric

$$ds^2 = dt^2 - a^2(t)\left[dr^2 + r^2\left(d\theta^2 + \sin^2\theta\, d\phi^2\right)\right], \tag{3}$$

where and (t, r, θ, ϕ) are comoving coordinates. The Friedmann equations take the form

$$3H^2 = \rho, \tag{4}$$

$$2\dot{H} + 3H^2 = -p, \tag{5}$$

where ρ is the total energy density, p is the total pressure, and we work in units with $8\pi G = c = 1$, where G is the Newtonian constant of gravitation and c is the speed of light. The conservation of the total energy–momentum tensor reads

$$\dot{\rho} + 3H(\rho + p) = 0. \tag{6}$$

We first consider a cosmological scenario with three fluids. The total energy density and pressure are written as

$$\rho = \epsilon\,\rho_1 + \rho_2 + \rho_x, \qquad p = \epsilon\, p_1 + p_2 + p_x, \tag{7}$$

where ρ_1 and ρ_2 are the energy densities of two ideal fluids satisfying $p_1 = \omega_1\rho_1$ and $p_2 = \omega_2\rho_2$, with $\omega_1 \neq \omega_2$ constant, and ρ_x is the holographic dark energy given by (2),

with $p_x = \omega\rho_x$ and, in general, a time-dependent equation of state ω. The parameter ϵ takes the integer values $\{0, 1\}$. Combining these ingredients, Equation (5) can be rewritten as

$$\epsilon\,\frac{\omega_1}{\omega_2}\rho_1 + \rho_2 = -3\left(\frac{\alpha\omega + 1}{\omega_2}\right)H^2 - \left(\frac{3\beta\omega + 2}{\omega_2}\right)\dot{H}. \tag{8}$$

In what follows, we analyze particular realizations of Equation (8).

2.1. Holographic Dark Energy and a Single Fluid

Here, we set $\epsilon = 0$ in Equation (8), so that ρ_2 can be written as a function $\rho_2(H^2, \dot{H}, \omega)$. Replacing ρ_2 from Equation (4) and ρ_x from Equation (2) into Equation (5), one obtains

$$\dot{H} = -3\left(\frac{\alpha(\omega - \omega_2) + \omega_2 + 1}{3\beta(\omega - \omega_2) + 2}\right)H^2. \tag{9}$$

Equation (9) can be integrated when ω is constant, but it has a non-trivial solution in the general case of a varying equation of state. Replacing Equation (9) into Equations (2) and (8), one finds [14]

$$\rho_x = 3H^2\left(\frac{2\alpha - 3\beta(\omega_2 + 1)}{3\beta(\omega - \omega_2) + 2}\right), \tag{10}$$

$$\rho_2 = \frac{2(1 - \alpha) + 3\beta(1 + \omega)}{2\alpha - 3\beta(1 + \omega_2)}\,\rho_x. \tag{11}$$

In this regime, and for the constant ω, the holographic component effectively tracks the auxiliary fluid ρ_2, so that the model does not provide a suitable description of late-time acceleration if both ρ_2 and ρ_x are interpreted as dark components.

To explore more general situations, we allow for an interaction between the two fluids. Introducing the variable $\eta = 3\ln a$ and denoting derivatives with respect to η by a prime, the conservation equations for the two components can be written as

$$\rho_2' + (1 + \omega_2)\rho_2 = -\Gamma, \tag{12}$$

$$\rho_x' + (1 + \omega)\rho_x = \Gamma, \tag{13}$$

where $\Gamma = Q/(3H)$ encodes the interaction term between ρ_2 and the holographic dark energy.

Holographic Dark Energy with Variable ω

From Equations (2)–(5) it follows that, in the absence of interaction, the equation of state is forced to be constant, with

$$\omega_2 = -1 + \frac{2}{3}\frac{\alpha}{\beta}, \qquad \omega = -1 + \frac{2}{3}\frac{\alpha - 1}{\beta}. \tag{14}$$

There are two natural ways of introducing a varying equation of state: (i) by specifying a time-dependent parameterization for ω [14] or (ii) by allowing for an interaction in the dark sector and inferring the implicit evolution of ω from the coupled dynamics.

Following the second approach, and in line with the earlier study [31], we consider interaction terms constructed from linear combinations of the component densities. In particular, we adopt the ansatz

$$\Gamma = b\,\rho_i, \tag{15}$$

where b is a coupling constant, and ρ_i is either ρ_2 or ρ_x.

2.1.1. Interaction Proportional to ρ_2

We first study the case $\Gamma = b\,\rho_2$. Equations (12) and (13) become

$$\rho_2' + (1 + \omega_2 + b)\rho_2 = 0, \tag{16}$$

$$\rho_x' + (1 + \omega)\rho_x - b\,\rho_2 = 0. \tag{17}$$

Integrating Equation (16), one obtains $\rho_2 \propto a^{-3(1+\omega_2+b)}$. Using this expression together with Equations (2) and (4), we derive a differential equation for H^2, whose solution reads

$$H^2 = \tilde{C}_1\, a^{-2(\alpha-1)/\beta} + \frac{2}{3\left[3\beta(1+\omega_2+b) - 2(\alpha-1)\right]}\,\rho_{20}\, a^{-3(1+\omega_2+b)}, \tag{18}$$

where $\tilde{C}_1$ is an integration constant, and

$$3\beta(1 + \omega_2 + b) - 2(\alpha - 1) \neq 0 \tag{19}$$

must hold. The corresponding holographic density, obtained from Equations (4) and (18), is

$$\rho_x = 3\,\tilde{C}_1\, a^{-2(\alpha-1)/\beta} + \frac{2\alpha - 3\beta(1+\omega_2+b)}{3\beta(1+\omega_2+b) - 2(\alpha-1)}\,\rho_{20}\, a^{-3(1+\omega_2+b)}. \tag{20}$$

Combining Equation (20) with the conservation Equation (17) allows us to solve for the time dependence of the equation of state $\omega(a)$. Alternatively, inserting Equation (18) into Equation (10) yields

$$\rho_x = 3\tilde{C}_1\left(\frac{2\alpha - 3\beta(1+\omega_2)}{3\beta(\omega-\omega_2)+2}\right)a^{-2(\alpha-1)/\beta} + \frac{2}{3\beta(1+\omega_2+b) - 2(\alpha-1)}\left(\frac{2\alpha - 3\beta(1+\omega_2)}{3\beta(\omega-\omega_2)+2}\right)\rho_{20}a^{-3(1+\omega_2+b)}. \tag{21}$$

Since the holographic density must be unique, comparing Equations (20) and (21) leads to the constraints

$$\frac{2\alpha - 3\beta(1+\omega_2)}{3\beta(\omega-\omega_2)+2} = 1, \tag{22}$$

$$3\beta(1 + \omega_2 + b) - 2(\alpha - 1) = 0. \tag{23}$$

Equation (22) implies that ω must be constant, while Equation (23) contradicts the requirement (19). Therefore, for two fluids ρ_2 and ρ_x, interacting through a term $Q \propto H\rho_2$, the holographic equation of state cannot be both dynamical and consistent with the assumed form of the energy densities. In particular, our findings are at odds with the behavior reported in Ref. [32], where an interaction $Q = 3Hb\rho_m$ between pressureless matter and holographic dark energy leads to a variable equation of state $\omega(\rho_m/\rho_x)$.

2.1.2. Interaction Proportional to ρ_x

We now take $\Gamma = b\,\rho_x$. The conservation equations become

$$\rho_2' + (1 + \omega_2)\rho_2 + b\,\rho_x = 0, \tag{24}$$

$$\rho_x' + (1 + \omega - b)\rho_x = 0. \tag{25}$$

Differentiating Equation (11) and using Equation (24), one obtains

$$\rho_x' + \left[\frac{3\beta\,\omega' + b(2\alpha - 3\beta(1+\omega_2))}{2(1-\alpha)+3\beta(1+\omega)} + 1 + \omega_2\right]\rho_x = 0. \tag{26}$$

Comparing Equations (25) and (26) yields the following differential equation for ω:

$$\omega' + A\,\omega - \omega^2 + B = 0, \tag{27}$$

with

$$A = \frac{2}{3\beta}(\alpha - 1) + \omega_2 + b - 1, \qquad B = \frac{2}{3\beta}\left[(1-\alpha)\omega_2 + b\right] + (1-b)\omega_2. \tag{28}$$

Provided $2(1-\alpha) + 3\beta(1+\omega) \neq 0$ and $\beta \neq 0$, Equation (27) admits the explicit solution

$$\omega(a) = \frac{1}{2}\left[A + \sqrt{-A^2 - 4B}\,\tan\left(\frac{1}{2}\sqrt{-A^2-4B}\,(3\ln a - C_1)\right)\right], \tag{29}$$

where C_1 is an integration constant. In this case, the interaction $\Gamma \propto \rho_x$ can induce a non-trivial evolution of the holographic equation of state.

Linear interactions between cold dark matter and holographic dark energy, typically of the form $Q \propto H\rho_m$ or $Q \propto H\rho_x$, have been explored in several studies [16,17,26,33]. In particular, Ref. [16] considered the three cases $Q \propto H\rho_x$, $Q \propto H\rho_m$, and $Q \propto H(\rho_x + \rho_m)$, deriving a second-order differential equation for $H(a)$ when $\epsilon = 0$ and using it to reconstruct the dynamics. In Ref. [17], interacting cold dark matter and holographic dark energy with $\omega = \omega(r)$, $r = \rho_c/\rho_x$, were studied, leading to interaction terms of the form $Q = Q(\rho, \rho')$ and explicit solutions for $\rho_i(a)$ and $\omega(a)$.

Nonlinear interactions have also been proposed. For instance, Ref. [18] analyzed a coupling $Q = 3Hb\,\rho_m^2/(\rho_m + \rho_x)$, which leads to a nonlinear second-order equation for $H^2(x)$, $x = \ln a$, and to a future Big Rip-type singularity in the holographic energy density. In Ref. [19], an interaction $Q = 3Hb\,\rho_x^2/(\rho_m + \rho_x)$ was considered, and the resulting $\omega(a)$ was reconstructed.

2.2. Holographic Dark Energy and Two Ideal Fluids

We now take $\epsilon = 1$ in Equations (4) and (8), which, together with Equation (2), yield

$$\rho_i = 3\left(\frac{\alpha(\omega - \omega_j) + \omega_j + 1}{\omega_j - \omega_i}\right)H^2 + \left(\frac{3\beta(\omega - \omega_j) + 2}{\omega_j - \omega_i}\right)\dot{H}, \tag{30}$$

for $i, j = \{1, 2\}$ and $i \neq j$. Both the auxiliary fluids and the holographic density now depend on H, $\dot{H}$, and ω.

2.2.1. Constant Holographic Equation of State

We first consider the case where all three fluids are non-interacting and have constant equations of state. The conservation Equation (6) splits into

$$\rho_1' + (1+\omega_1)\rho_1 = 0, \tag{31}$$

$$\rho_2' + (1+\omega_2)\rho_2 = 0, \tag{32}$$

$$\rho_x' + (1+\omega)\rho_x = 0. \tag{33}$$

Integrating Equations (31) and (32) and inserting the solutions into Equation (30), one obtains a differential equation for H^2, whose solution can be written as

$$H^2 = A\, a^{-3(1+\omega_1)} + B\, a^{-3(1+\omega_2)}, \tag{34}$$

with A and B constants. On the other hand, using the solution of Equation (33) in Equation (2) gives

$$H^2 = \frac{2\rho_{x0}}{3\big(2\alpha - 3\beta(1+\omega)\big)}\, a^{-3(1+\omega)} + \bar{C}_3\, a^{-2\alpha/\beta}, \tag{35}$$

where $\bar{C}_3$ is an integration constant. Comparing Equations (34) and (35), one finds

$$-3(1+\omega_1) = -3(1+\omega), \qquad -3(1+\omega_2) = -2\frac{\alpha}{\beta}, \tag{36}$$

or the same system with ω_1 and ω_2 exchanged, so that

$$\omega = \omega_1 \quad \text{or} \quad \omega = \omega_2. \tag{37}$$

Therefore, as long as the components do not interact and all equations of state are constant, the holographic dark energy emulates one of the ideal fluids.

A particularly relevant case is obtained by choosing $\rho_1 = \rho_f$, with $\omega_1 = \omega_f$, $\rho_2 = \rho_m$, with $p_2 = p_m = 0$, and ρ_x as the holographic dark energy. Then, $\omega \in \{0, \omega_f\}$, and the holographic component mimics either dust or a general fluid. In the context of standard cosmology, this fluid could be either radiation ($\omega_r = 1/3$) or baryons ($\omega_b = 0$). In both cases, the resulting dynamics does not account for a late-time accelerated expansion.

2.2.2. Interaction in the Dark Sector

We now consider a different setup in which fluid 1 does not interact with the other components, while fluid 2 and the holographic dark energy may exchange energy. The conservation Equation (6) becomes

$$\rho_1' + (1+\omega_1)\rho_1 = 0, \tag{38}$$
$$\rho_2' + (1+\omega_2)\rho_2 = -\Gamma, \tag{39}$$
$$\rho_x' + (1+\omega)\rho_x = \Gamma. \tag{40}$$

Integrating Equation (38) and inserting the result into Equation (30) for ρ_1 yields a differential equation for H^2 with solution

$$\begin{aligned} H^2 = {} & \frac{2\rho_{10}(\omega_2 - \omega_1)}{3\big[2(\omega_2 - \omega_1) + (2\alpha - 3\beta(1+\omega_1))(\omega - \omega_2)\big]}\, a^{-3(1+\omega_1)} \\ & + \bar{C}\, a^{-6\left[\frac{1+\alpha(\omega-\omega_2)+\omega_2}{2+3\beta(\omega-\omega_2)}\right]}, \end{aligned} \tag{41}$$

where $\bar{C}$ is an integration constant. Using Equations (2) and (41) in Equation (40), we obtain

$$\Gamma(a) = \bar{\alpha}\, a^{-3(1+\omega_1)} + \bar{\beta}\, a^{-6\left[\frac{1+\alpha(\omega-\omega_2)+\omega_2}{2+3\beta(\omega-\omega_2)}\right]}, \tag{42}$$

with $\bar{\alpha}$ and $\bar{\beta}$ constant. Substituting Equation (42) into Equations (39) and (40) leads to

$$\rho_2 = \bar{C}_2\, a^{-3(1+\omega_2)} + \frac{\bar{\alpha}}{3(\omega_1-\omega_2)} a^{-3(1+\omega_1)} + \frac{\bar{\beta}\big(2+3\beta(\omega-\omega_2)\big)}{3(\omega-\omega_2)\big(2\alpha-3\beta(1+\omega_2)\big)} a^{-6\left[\frac{1+\alpha(\omega-\omega_2)+\omega_2}{2+3\beta(\omega-\omega_2)}\right]}, \tag{43}$$

$$\rho_x = \bar{C}_x\, a^{-3(1+\omega)} + \frac{\bar{\alpha}}{3(\omega-\omega_1)} a^{-3(1+\omega_1)} + \frac{\bar{\beta}\big(2+3\beta(\omega-\omega_2)\big)}{3(\omega-\omega_2)\big(2-2\alpha+3\beta(1+\omega)\big)} a^{-6\left[\frac{1+\alpha(\omega-\omega_2)+\omega_2}{2+3\beta(\omega-\omega_2)}\right]}, \tag{44}$$

where $\bar{C}_2$ and $\bar{C}_x$ are integration constants.

A scenario of particular cosmological interest arises when fluid 1 is identified with baryons, $\rho_1 = \rho_b$, with $p_1 = p_b = 0$, and fluid 2 with cold dark matter, $\rho_2 = \rho_m$, with $p_2 = p_m = 0$, while ρ_x is the holographic dark energy. In this case, the baryons remain non-interacting, $\rho_b \propto a^{-3}$, and the interacting dark sector is formed by ρ_m and ρ_x. From Equations (43) and (44), we obtain densities of the general form $\rho_i = \bar{\alpha}_i\, a^{-3(1+\omega_i)} + \bar{\beta}_i\, a^{-6[(1+\alpha\omega)/(2+3\beta\omega)]}$, where i labels dark matter or holographic dark energy. In this regime, the interaction term behaves as $\Gamma \propto a^{-6[(1+\alpha\omega)/(2+3\beta\omega)]}$ or, equivalently, as a linear combination $\Gamma = \tilde{\alpha}\rho_b + \tilde{\beta}\rho_m$.

3. Current Scenario with Holographic Dark Energy

We now turn to a more realistic configuration that includes the standard cosmological components: baryons, radiation, cold dark matter, and holographic dark energy. We again consider a flat FLRW universe governed by Equations (4) and (6), with

$$\rho = \rho_b + \rho_r + \rho_c + \rho_x, \qquad p = p_b + p_r + p_c + p_x, \tag{45}$$

and define the dark sector as $\rho_d := \rho_c + \rho_x$. Each fluid obeys a barotropic equation of state $p_i = \omega_i \rho_i$, with $\omega_b = 0$, $\omega_r = 1/3$, $\omega_c = 0$, and $\omega_x = \omega$.

Allowing for a phenomenological interaction in the dark sector, the conservation Equation (6) splits into

$$\rho_b' + \rho_b = 0, \tag{46}$$

$$\rho_r' + \frac{4}{3}\rho_r = 0, \tag{47}$$

$$\rho_c' + \rho_c = -\Gamma, \tag{48}$$

$$\rho_x' + (1+\omega)\rho_x = \Gamma, \tag{49}$$

where $\Gamma = Q/(3H)$ now encodes the interaction between cold dark matter and holographic dark energy.

For Ricci-type holographic dark energy with $\beta = 0$, Equation (2) reduces to [12]

$$\rho_x = \alpha\, \rho, \tag{50}$$

with $\rho = \rho_b + \rho_r + \rho_d$. Integrating Equations (46) and (47) yields

$$\rho_b = \rho_{b0}\, a^{-3}, \qquad \rho_r = \rho_{r0}\, a^{-4}. \tag{51}$$

Using these expressions and the relation $\rho_c = \rho_d - \rho_x$ in Equation (48) and differentiating Equation (50), one obtains checked and confirmed the correction and suggestion. a first-order differential equation for the dark sector:

$$(\alpha - 1)\rho_d' + (\alpha - 1)\rho_d - \frac{\alpha}{3}\rho_{r0}\, a^{-4} = \Gamma. \tag{52}$$

Similar to that in Section 2, we consider three types of linear interactions [30,34–37], defined as

$$\begin{aligned} \Gamma_1 &= \alpha_1\rho_c + \beta_1\rho_x \qquad \text{(Model 1)}, \\ \Gamma_1 &= \alpha_1\rho_c + \beta_1\rho_x \qquad \text{(Model 2)}, \\ \Gamma_1 &= \alpha_1\rho_c + \beta_1\rho_x \qquad \text{(Model 3)}. \end{aligned} \tag{53}$$

These interactions can be expressed in terms of combinations of ρ_d, ρ_d', ρ, and ρ', so that Equation (52) can be recast as

$$\rho_d' + b_1\rho_d + b_2 a^{-3} + b_3 a^{-4} = 0, \tag{54}$$

where the constants b_1, b_2, and b_3 depend on the interaction parameters. The general solution of Equation (54) reads

$$\rho_d(a) = \frac{b_2}{1 - b_1} a^{-3} + \frac{3b_3}{4 - 3b_1} a^{-4} + C\, a^{-3b_1}, \tag{55}$$

with C an integration constant.

The explicit expressions for b_1, b_2, and b_3 in each interaction scheme are as follows.

- For Γ_1,

$$b_1 = 1 - \frac{\alpha_1 + \alpha(\beta_1 - \alpha_1)}{\alpha - 1}, \quad b_2 = \frac{\alpha(\alpha_1 - \beta_1)}{\alpha - 1}\rho_{b0}, \quad b_3 = \frac{\alpha\left[3(\alpha_1 - \beta_1) - 1\right]}{3(\alpha - 1)}\rho_{r0}.$$

- For Γ_2,

$$b_1 = \frac{\alpha - 1}{\alpha(1 - \beta_2 + \alpha_2) - \alpha_2 - 1}, \quad b_2 = \frac{\alpha(\beta_2 - \alpha_2)}{\alpha(1 - \beta_2 + \alpha_2) - \alpha_2 - 1}\rho_{b0},$$

$$b_3 = \frac{\alpha\left[4(\beta_2 - \alpha_2) - 1\right]}{3\left[\alpha(1 - \beta_2 + \alpha_2) - \alpha_2 - 1\right]}\rho_{r0}.$$

- For Γ_3,

$$b_1 = \frac{\alpha - 1 - \alpha_3}{\alpha - 1 - \beta_3}, \quad b_2 = 0, \quad b_3 = -\frac{\alpha}{3(\alpha - 1 - \beta_3)}\rho_{r0}.$$

The constant C can be written in terms of present-day quantities as

$$C = 3H_0^2(\Omega_{c0} + \Omega_{x0}) - \frac{b_2}{1 - b_1} - \frac{3b_3}{4 - 3b_1}, \tag{56}$$

where H_0, Ω_{c0}, and Ω_{x0} are the current values of the Hubble parameter and the density parameters for cold dark matter and holographic dark energy, respectively.

The holographic equation of state can be obtained from

$$\omega = \frac{\Gamma - \alpha\rho'}{\alpha\rho} - 1, \tag{57}$$

using the solution (55) and Equation (51) for each interaction scheme. In all cases, the result can be written as

$$\omega(a) = \frac{E_1 a^{-3} + E_2 a^{-4} + E_3 a^{-3b_1}}{\bar{A} a^{-3} + \bar{B} a^{-4} + \bar{C} a^{-3b_1}} - 1, \tag{58}$$

where

$$\bar{A} = \alpha\left(\rho_{b0} + \frac{b_2}{1-b_1}\right), \quad \bar{B} = \alpha\left(\rho_{r0} + \frac{3b_3}{4-3b_1}\right), \quad \bar{C} = \alpha\, C, \tag{59}$$

and the coefficients E_i ($i = 1, 2, 3$) are linear combinations of the interaction parameters associated with each model. In the asymptotic future, $a \to \infty$, and for $b_1 < 0$, Equation (58) approaches

$$\omega_\infty = \frac{E_3}{\bar{C}} - 1, \tag{60}$$

indicating that the interacting holographic dark energy tends to an effective constant equation of state.

To examine the coincidence problem, we consider the ratio $r = \rho_c/\rho_x$. Using Equations (51) and (55), we compute $r(a)$ and evaluate its asymptotic value as $a \to \infty$. For all the interactions considered here with $b_1 < 0$, the coincidence parameter converges to a constant, which, remarkably, does not depend on the interaction parameters.

4. Observational Analysis and Results

In this Section, we confront the interacting Ricci-type holographic dark energy scenarios with observational data at the background level. We consider two complementary probes: cosmic chronometers (CC), which provide direct information on the Hubble expansion rate $H(z)$ as a funcction of redshift z, and Type Ia supernovae, which constrain the luminosity distance–redshift relation.

4.1. Cosmic Chronometers

Cosmic chronometers are based on the differential age method applied to passively evolving early-type galaxies [38]. Following the strategy of Ref. [39], the relative ages of galaxy populations at different redshifts are used to estimate dz/dt, which in turn yields the Hubble parameter through

$$H(z) = -\frac{1}{1+z}\frac{dz}{dt}. \tag{61}$$

The values employed here are derived from the BC03 (Bruzual–Charlot 2003) stellar population synthesis models [40] and provide cosmology-independent measurements of the expansion history [41]. In our analysis, we restrict the CC data to redshifts $z \lesssim 1.2$, where the method is most robust.

The theoretical Hubble function $H(z)$ is obtained from Equations (4), (51) and (55), using $a = (1+z)^{-1}$. Figure 1 displays the CC data points together with the best fit curves for the three interacting holographic models and the ΛCDM reference model.

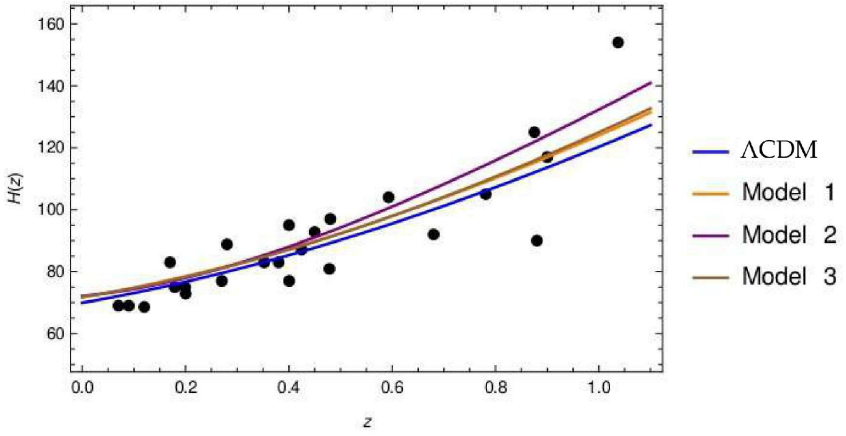

Figure 1. Hubble expansion rate for the concordance ΛCDM model and for the interacting Ricci-type holographic dark energy scenarios (53). The solid dots correspond to cosmic chronometer measurements [40,41] of $H(z)$ up to $z \simeq 1.2$ redshifts.

It is worth emphasizing that, within the interacting Ricci-type holographic dark energy scenarios considered in this paper, the cosmic acceleration is not assumed to be positive at all epochs. As in the standard cosmological picture, the models naturally accommodate an early decelerated expansion phase dominated by radiation and matter, followed by a late-time accelerated regime driven by the dark energy component. This behavior can be inferred from the evolution of the Hubble function $H(z)$ and from the corresponding effective equation of state of the dark energy sector. In particular, at high ($z \gtrsim 0.6$) redshifts the contribution of radiation and pressureless matter ensures a decelerated expansion, while at low ($z \lesssim 0.6$) redshifts, the holographic dark energy becomes dominant and leads to a negative effective pressure, giving rise to accelerated expansion. The interacting models analyzed here, therefore, reproduce the expected transition from deceleration to acceleration without requiring fine-tuning. Consequently, the present acceleration is a late-time phenomenon in these scenarios, consistent with observational evidence, rather than a feature that persists throughout the entire cosmic history.

4.2. Type Ia Supernovae

As a complementary background probe, we use the Pantheon sample of Type Ia supernovae (SNe Ia) [42], which consists of 1048 spectroscopically confirmed SNe Ia in the redshift range $0.01 \leq z \leq 2.3$. The catalog provides peak magnitudes in the rest-frame B-band, m_B, from which the

$$\mu = m_B + M_B, \tag{62}$$

where M_B is a nuisance parameter corresponding to the absolute magnitude of a fiducial supernova. In our analysis, the theoretical distance modulus at redshift z is computed as

$$\mu(z) = 5 \log_{10} d_L(z) + 25, \tag{63}$$

with the luminosity distance given by

$$d_L(z) = (1+z) \int_0^z \frac{H_0 \, dz'}{H(z')} \quad [\text{Mpc}]. \tag{64}$$

We perform a joint analysis combining the CC data set and the Pantheon SNe Ia sample, following the statistical treatment described in Ref. [30].

Table 1 summarizes the best fit values for the Hubble parameter $h = H_0/(100\,\mathrm{km\,s^{-1}\,Mpc^{-1}})$, the present cold dark matter density parameter Ω_c, and the parameters α, α_1, and β_1 characterizing the interacting holographic models under consideration, together with the corresponding values for the ΛCDM model used as reference.

Table 1. Best fit values for the parameters of the studied models, using the cosmic chronometer data set [40,41] combined with the Pantheon SNe Ia sample [42]. See text for details.

Model	h	Ω_c	α	α_1	β_1
ΛCDM	$0.6993^{+0.0077}_{-0.0095}$	$0.234^{+0.011}_{-0.0096}$	—	—	—
Model 1	0.717 ± 0.011	0.378 ± 0.052	$0.901^{+0.079}_{-0.043}$	—	-0.090 ± 0.038
Model 2	$0.7216^{+0.0068}_{-0.0089}$	$0.1734^{+0.0091}_{-0.014}$	$0.828^{+0.037}_{-0.031}$	$-0.0836^{+0.015}_{-0.0086}$	—
Model 3	$0.7184^{+0.0088}_{-0.012}$	$0.248^{+0.039}_{-0.079}$	$0.943^{+0.054}_{-0.019}$	$0.023^{+0.016}_{-0.023}$	$0.023^{+0.016}_{-0.023}$

Figures 2–4 show the two-dimensional marginalized constraints for the interacting models (53), with contours corresponding to the 68.3% and 95.4% confidence levels. The plots illustrate that the interaction parameters are moderately constrained by the combined data and that the resulting cosmologies provide a reasonable fit to the CC [40,41] and SNe Ia [42] observations, remaining close to the ΛCDM reference.

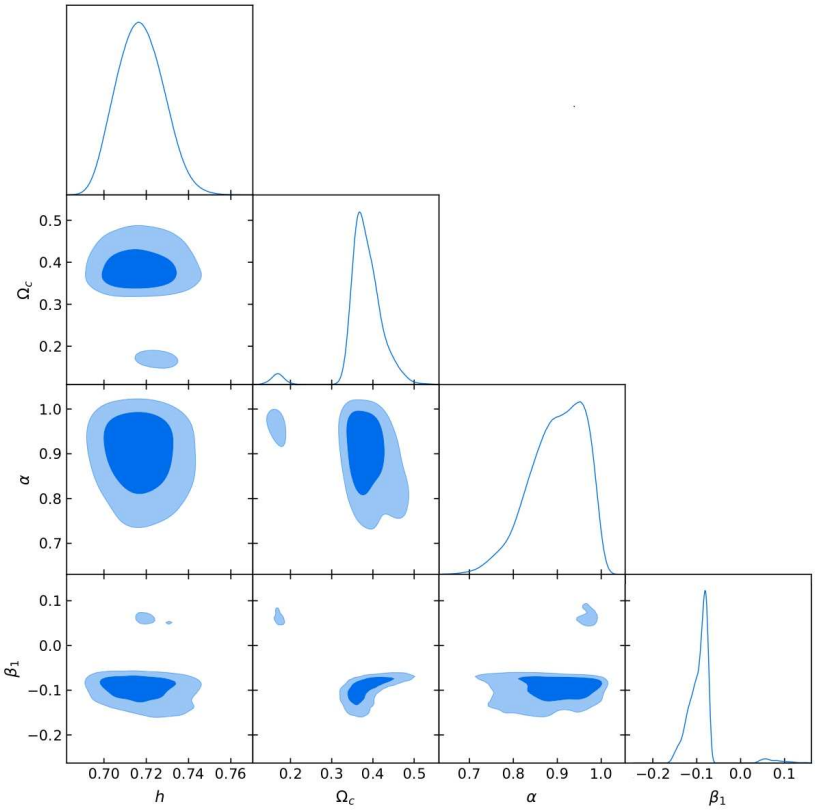

Figure 2. Contour plots for the parameters of interaction Model 1, showing the 1σ (one standard deviation, light blue) and 2σ (dark blue) confidence regions from the joint analysis of cosmic chronometers [40,41]and Pantheon SNe Ia [42] data.

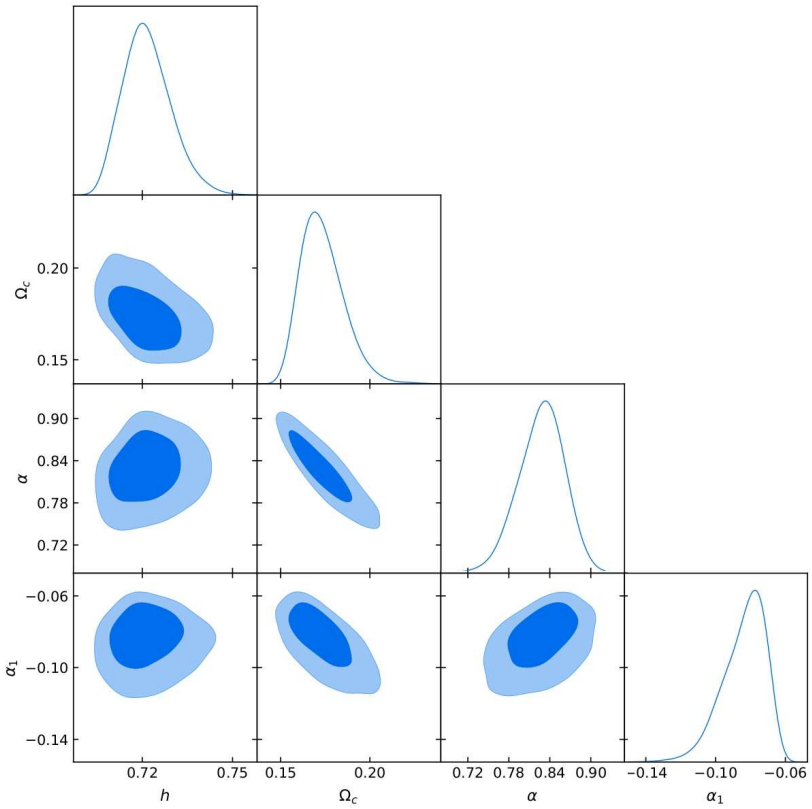

Figure 3. Same as Figure 2, but for interaction Model 2.

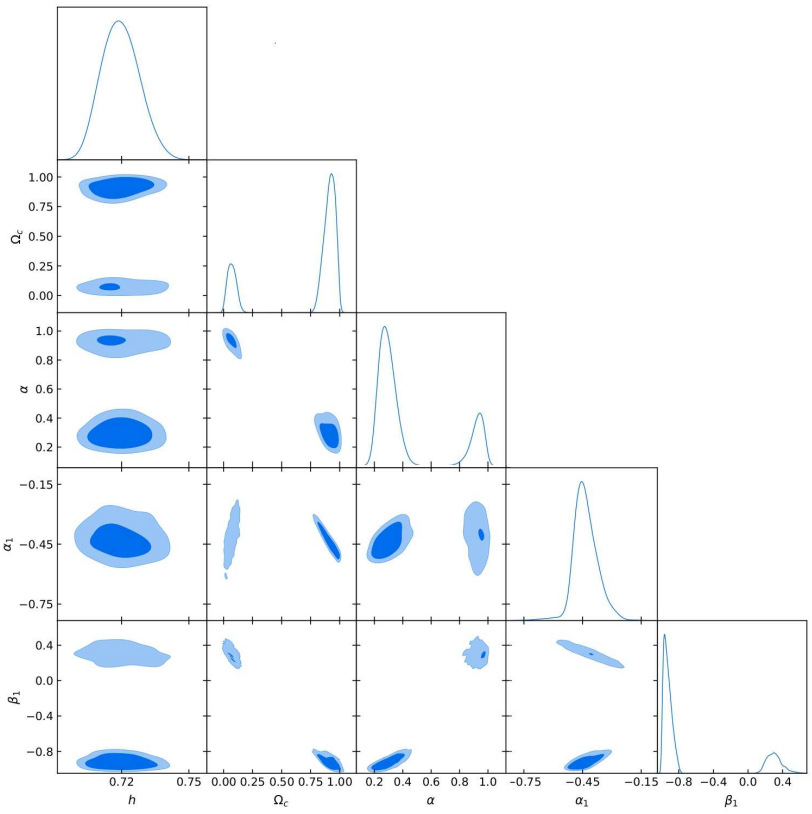

Figure 4. Same as Figure 2, but for interaction Model 3.

Several studies have already analyzed the performance of Ricci-type holographic dark energy models in comparison with ΛCDM. In particular, Ref. [43] considered non-interacting Ricci-type holographic dark energy and found that this model is disfavored

by data when confronted with ΛCDM. In Ref. [12], the interacting Ricci-type model was tested using information criteria (AIC and BIC) and also disfavored. A similar conclusion was reached in Ref. [44] for a modified Ricci-type holographic model without interaction. Ref. [45] studied several interacting Ricci-type models, finding that they are ruled out with respect to ΛCDM according to the BIC. Finally, in Ref. [46], both Ricci-type and modified Ricci-type holographic models without interaction were compared to ΛCDM using growth rate data in addition to background constraints, again yielding strong evidence against the holographic scenarios.

In case considered here, we find that the linear interacting Ricci-type models analyzed here can provide a background evolution that closely approximates that of ΛCDM (see Table 1 and Figure 1), while allowing for a dynamical equation of state and a non-trivial asymptotic behavior of the coincidence parameter. A detailed statistical comparison using information criteria and structure growth data is left for our future work.

5. Conclusions

In this paper, we have investigated cosmological scenarios in which the late-time dynamics of the Universe is driven by a Ricci-type holographic dark energy component interacting with cold dark matter. Starting from a spatially flat FLRW background within General Relativity, we first revisited simplified configurations involving one or two ideal fluids in addition to the holographic component. In these setups, we showed that, for constant equations of state and in the absence of interaction, the holographic energy density tends to emulate one of the auxiliary fluids and therefore fails to produce a genuine accelerated expansion. We also analyzed under which conditions a variable holographic equation of state can be obtained through a suitable interaction term.

We then focused on a more realistic four-fluid scenario including baryons, radiation, cold dark matter, and holographic dark energy. In this context, we introduced three phenomenological interaction schemes in the dark sector, denoted by Γ_1, Γ_2, and Γ_3, and derived analytic solutions for the total dark sector energy density and for the holographic equation of state. In all three cases, the dark sector density can be expressed as a linear combination of power laws in the scale factor, and the equation of state takes the general form of Equation (58). For models with $b_1 < 0$, we showed that the holographic equation of state approaches a constant value in the asymptotic future and that the coincidence parameter $r = \rho_c/\rho_x$ converges to a constant limit independent of the interaction parameters. This behavior offers a possible alleviation of the coincidence problem.

To confront the models with observations, we have considered background data from cosmic chronometers, which directly constrain the Hubble expansion rate $H(z)$, and the Pantheon sample of Type Ia supernovae, which probes the luminosity distance–redshift relation. Performing a joint analysis, we obtained the best fit values for the cosmological and interaction parameters in the three interacting models and in the ΛCDM reference (Table 1). We found that the interacting Ricci-type holographic models provide a good fit to the data and closely track the background evolution of ΛCDM (Figure 1), while introducing a non-trivial dark sector coupling and a dynamical dark energy equation of state. The two-dimensional marginalized constraints for each model (Figures 2–4) show that the interaction parameters are moderately constrained by the combined data sets.

Our analysis is restricted to background observables. The earlier studies have reported strong tensions between Ricci-type holographic models and ΛCDM when information criteria or structure growth data are taken into account [12,43–46]. In this sense, the interacting Ricci-type models presented here should be subjected to a similar scrutiny, including the analysis of linear perturbations, matter power spectra, and redshift–space distortions. It would also be of interest to explore whether alternative interaction forms or

generalized holographic cutoffs can further improve the observational performance of these scenarios while maintaining their appealing connection with the holographic principle.

Let us note that the cosmological parameters inferred from background observables in this study can also be confronted with complementary probes that are weakly dependent on the Hubble constant, such as galaxy cluster mass measurements. A fully quantitative comparison with such observables would require extending the present background-level analysis to include the growth of cosmic structures, which is left for future work.

More broadly, our results illustrate how holographic dark energy models with dark sector interactions can mimic the concordance model at the background level while offering a richer phenomenology for the late-time dynamics of the Universe. Future observational surveys and a combined analysis of background and perturbation data will be crucial to clarify whether such interacting holographic scenarios can survive as viable competitors to ΛCDM.

Author Contributions: Conceptualization, C.R.-B. and S.S.-M.; methodology, N.M.-Z. and K.L.-B.; formal analysis, A.C.-B., C.N.-C. and M.G.-H.; investigation, F.M.-G., V.V.-L. and M.B.-C.; writing—original draft preparation, C.R.-B., S.S.-M., A.C.-B., and C.N.-C.; writing—review and editing, M.G.-H., V.V.-L., M.B.-C. and A.R.-M.; supervision, N.M.-Z. and K.L.-B.; project administration, C.R.-B., F.M.-G. and A.R.-M.; funding acquisition, C.R.-B. All authors have read and agreed to the published version of the manuscript.

Funding: This research was funded by CONCYTEC via the PROCIENCIA program under project PE501082885-2023 and by the Universidad Nacional de Trujillo, Peru, through Resolución Rectoral No. 0369-2022/UNT (PIC No. 01-2021-MOD.04).

Data Availability Statement: The original contributions presented in this study are included in the article; further inquiries can be directed to the corresponding author.

Acknowledgments: The authors thank the members of the consolidated research group GRACOCC (Gravitación, Cosmología, Campos y Cuerdas) at the Universidad Nacional de Trujillo, Peru, for fruitful discussions and continuous support.

Conflicts of Interest: The authors declare no conflicts of interest.

References

1. Riess, A.G.; Filippenko, A.V.; Challis, P.; Clocchiatti, A.; Diercks, A.; Garnavich, P.M.; Gilliland, R.L.; Hogan, C.J.; Jha, S.; Kirshner, R.P.; et al. Observational evidence from supernovae for an accelerating universe and a cosmological constant. *Astron. J.* **1998**, *116*, 1009. [CrossRef]
2. Perlmutter, S.; Aldering, G.; Goldhaber, G.; Knop, R.A.; Nugent, P.; Castro, P.G.; Deustua, S.; Fabbro, S.; Goobar, A.; Groom, D.E.; et al. [The Supernova Cosmology Project] Measurements of Ω and Λ from 42 high-redshift supernovae. *Astrophys. J.* **1999**, *517*, 565–686. [CrossRef]
3. Spergel, D.N.; Bean, R.; Doré, O.; Nolta, M.R.; Bennett, C.L.; Dunkley, J.; Hinshaw, G.; Jarosik, N.; Komatsu, E.; Page, L.; et al. Three-year *Wilkinson Microwave Anisotropy Probe (WMAP)* observations: Implications for cosmology. *Astrophys. J. Suppl. Ser.* **2007**, *170*, 377–408. [CrossRef]
4. Ade, P.A.R.; Aghanim, N.; Arnaud, M.; Ashdown, M.; Aumont, J.; Baccigalupi, C.; Banday, A.J.; Barreiro, R.B.; Bartlett, J.G.; Bartolo, N.; et al. [Planck Collaboration] *Planck* 2015 results. XIII. Cosmological parameters. *Astron. Astrophys.* **2016**, *594*, A13. [CrossRef]
5. Weller, J.; Lewis, A.M. Large-scale cosmic microwave background anisotropies and dark energy. *Mon. Not. R. Astron. Soc.* **2003**, *346*, 987–993. [CrossRef]
6. Copeland, E.J.; Sami, M.; Tsujikawa, S. Dynamics of dark energy. *Int. J. Mod. Phys. D* **2006**, *15*, 1753–1935. [CrossRef]
7. Riess, A.G.; Macri, L.M.; Hoffmann, S.L.; Scolnic, D.; Casertano, S.; Filippenko, A.V.; Tucker, B.E.; Reid, M.J.; Jones, D.O.; Silverman, J.M.; et al. A 2.4% determination of the local value of the Hubble constant. *Astrophys. J.* **2016**, *826*, 56. [CrossRef]
8. Riess, A.G.; Macri, L.; Casertano, S.; Lampeitl, H.; Ferguson, H.C.; Filippenko, A.V.; Jha, S.W.; Li, W.; Chornock, R. A 3% solution: determination of the Hubble constant with the *Hubble Space Telescope* and Wide Field Camera 3. *Astrophys. J.* **2011**, *730*, 119. [CrossRef]

9. Granda, L.N.; Oliveros, A. Infrared cut-off proposal for the holographic density. *Phys. Lett. B* **2008**, *669*, 275–277. [CrossRef]
10. Gao, C.; Wu, F.; Chen, X.; Shen, Y.-G. Holographic dark energy model from Ricci scalar curvature. *Phys. Rev. D* **2009**, *79*, 043511. [CrossRef]
11. Zhang, X. Holographic Ricci dark energy: Current observational constraints, quintom feature, and the reconstruction of scalar-field dark energy. *Phys. Rev. D* **2009**, *79*, 103509. [CrossRef]
12. Del Campo, S.; Fabris, J.C.; Herrera, R.; Zimdahl, W. Holographic dark-energy models. *Phys. Rev. D* **2011**, *83*, 123006. [CrossRef]
13. Lepe, S.; Peña, F. Crossing the phantom divide with Ricci-like holographic dark energy. *Eur. Phys. J. C* **2010**, *69*, 575–579. [CrossRef]
14. Arévalo, F.; Cifuentes, P.; Lepe, S.; Peña, F. Interacting Ricci-like holographic dark energy. *Astrophys. Space Sci.* **2014**, *352*, 899–907. [CrossRef]
15. Li, E.-K.; Zhang, Y.; Geng, J.-L.; Duan, P.-F. A bound system in the expanding universe with modified holographic Ricci dark energy and dark matter. *Astrophys. Space Sci.* **2015**, *355*, 187–193. [CrossRef]
16. Fu, T.-F.; Zhang, J.-F.; Chen, J.-Q.; Zhang, X. Holographic Ricci dark energy: Interacting model and cosmological constraints. *Eur. Phys. J. C* **2012**, *72*, 1932. [CrossRef]
17. Chimento, L.P.; Forte, M.I.; Richarte, M.G. Holographic dark energy linearly interacting with dark matter. *AIP Conf. Proc.* **2012**, *1471*, 39–44. [CrossRef]
18. Oliveros, A. Evolución cosmológica de un modelo de energía oscura con interacción no lineal. *Cienc. Desarro.* **2016**, *7*, 63–69. [CrossRef]
19. Oliveros, A.; Acero, M.A. New holographic dark energy model with non-linear interaction. *Astrophys. Space Sci.* **2015**, *357*, 12. [CrossRef]
20. Maldacena, J. The large-*N* limit of superconformal field theories and supergravity. *Int. J. Theor. Phys.* **1999**, *38*, 1113–1133. [CrossRef]
21. Fischler, W.; Susskind, L. Holography and cosmology. *arXiv* **1998**, arXiv:hep-th/9806039. [CrossRef]
22. Bousso, R. The holographic principle. *Rev. Mod. Phys.* **2002**, *74*, 825–874. [CrossRef]
23. 't Hooft, G. Dimensional reduction in quantum gravity. *arXiv* **1993**, arXiv:gr-qc/9310026. [CrossRef]
24. Susskind, L. The world as a hologram. *J. Math. Phys.* **1995**, *36*, 6377–6396. [CrossRef]
25. Bekenstein, J.D. Entropy bounds and black hole remnants. *Phys. Rev. D* **1994**, *49*, 1912–1921. [CrossRef]
26. Mathew, T.K.; Suresh, J.; Divakaran, D. Modified holographic Ricci dark energy model and statefinder diagnosis in flat universe. *Int. J. Mod. Phys. D* **2013**, *22*, 1350056. [CrossRef]
27. Pankunni, P.; Mathew, T.K. Interacting modified holographic Ricci dark energy model and statefinder diagnosis in flat universe. *Int. J. Mod. Phys. D* **2014**, *23*, 1450024. [CrossRef]
28. Rodríguez Benites, C.E. *Cosmologías con Expansión Acelerada*; Universidad del Bió Bió: Concepción, Chile, 2019. Available online: https://repositorio.concytec.gob.pe/handle/20.500.12390/2226 (accessed on 3 February 2026).
29. Rodriguez-Benites, C.; Cataldo, M.; Vásquez-Arteaga, M. Universe with holographic dark energy/Universo con energía oscura holográfica. *Rev. Fís. Momento* **2020**, *61*, 1–10. [CrossRef]
30. Cid, A.; Rodriguez-Benites, C.; Cataldo, M.; Casanova, G. Bayesian comparison of interacting modified holographic Ricci dark energy scenarios. *Eur. Phys. J. C* **2021**, *81*, 31. [CrossRef]
31. Cataldo, M.; Arevalo, F.; Minning, P. On a class of scaling FRW cosmological models. *J. Cosmol. Astropart. Phys.* **2010**, *2*, 24. [CrossRef]
32. Chattopadhyay, S.; Pasqua, A. Various aspects of interacting modified holographic Ricci dark energy. *Indian J. Phys.* **2013**, *87*, 1053–1057. [CrossRef]
33. Mahata, N.; Chakraborty, S. A dynamical system analysis of holographic dark energy models with different IR cutoff. *Mod. Phys. Lett. A* **2015**, *30*, 1550134. [CrossRef]
34. Arévalo, F.; Cid, A.; Moya, J. AIC and BIC for cosmological interacting scenarios. *Eur. Phys. J. C* **2017**, *77*, 565. [CrossRef]
35. Cid, A.; Santos, B.; Pigozzo, C.; Ferreira, T.; Alcaniz, J. Bayesian comparison of interacting scenarios. *J. Cosmol. Astropart. Phys.* **2019**, *3*, 30. [CrossRef]
36. Rodriguez-Benites, C.; Gonzalez-Espinoza, M.; Otalora, G.; Alva-Morales, M. Revisiting the dynamics of interacting vector-like dark energy. *Eur. Phys. J. C* **2024**, *84*, 276. [CrossRef]
37. Rodriguez-Benites, C.; Gonzalez-Espinoza, M.; Otalora, G.; Alva-Morales, M. Cosmological dynamics in interacting scalar-torsion $f(T,\phi)$ gravity: Investigating energy and momentum couplings. *Phys. Rev. D* **2025**, *111*, 043506. [CrossRef]
38. Moresco, M.; Pozzetti, L.; Cimatti, A.; Jimenez, R.; Maraston, C.; Verde, L.; Thomas, D.; Citro, A.; Tojeiro, R.; Wilkinson, D. A 6% measurement of the Hubble parameter at $z \sim 0.45$: Direct evidence of the epoch of cosmic re-acceleration. *J. Cosmol. Astropart. Phys.* **2016**, *5*, 14. [CrossRef]
39. Jimenez, R.; Loeb, A. Constraining cosmological parameters based on relative galaxy ages. *Astrophys. J.* **2002**, *573*, 37–42. [CrossRef]

40. Bruzual, G.; Charlot, S. Stellar population synthesis at the resolution of 2003. *Mon. Not. R. Astron. Soc.* **2003**, *344*, 1000–1028. [CrossRef]
41. Verde, L.; Protopapas, P.; Jimenez, R. The expansion rate of the intermediate universe in light of Planck. *Phys. Dark Universe* **2014**, *5*, 307–314. [CrossRef]
42. Scolnic, D.M.; Jones, D.O.; Rest, A.; Pan, Y.-C.; Chornock, R.; Foley, R.J.; Huber, M.E.; Kessler, R.; Narayan, G.; Riess, A.G.; et al. The complete light-curve sample of spectroscopically confirmed SNe Ia from Pan-STARRS1 and cosmological constraints from the combined Pantheon sample. *Astrophys. J.* **2018**, *859*, 101. [CrossRef]
43. Li, M.; Li, X.-D.; Wang, S.; Zhang, X. Holographic dark energy models: A comparison from the latest observational data. *JJ. Cosmol. Astropart. Phys.* **2009**, *6*, 36. [CrossRef]
44. Wang, Y.; Xu, L. Current observational constraints to the holographic dark energy model with a new infrared cutoff via the Markov chain Monte Carlo method. *Phys. Rev. D* **2010**, *81*, 083523. [CrossRef]
45. Feng, L.; Zhang, X. Revisit of the interacting holographic dark energy model after Planck 2015. *J. Cosmol. Astropart. Phys.* **2016**, *8*, 72. [CrossRef]
46. Akhlaghi, I.A.; Malekjani, M.; Basilakos, S.; Haghi, H. Model selection and constraints from holographic dark energy scenarios. *Mon. Not. R. Astron. Soc.* **2018**, *477*, 3659–3671. [CrossRef]